View metadata, citation and similar papers at core.ac.uk

brought to you by CORE

provided by Flinders Academic Commons

Flinders UNIVERSITY

Archived at the Flinders Academic Commons:

http://dspace.flinders.edu.au/dspace/

This is the publisher's copyright version of this article.

The original can be found at:

http://dx.doi.org/**DOI: 10.1117/12.759377**

Khung, Y.l., Cole, M.A., McInnes, S.J.P., and Voelcker, N.H. "Control over wettability via surface modification of porous gradients", Proceedings SPIE, 6799(679909) (2007).

Copyright 2007 Society of Photo-Optical Instrumentation Engineers. One print or electronic copy may be made for personal use only. Systematic reproduction and distribution, duplication of any material in this paper for a fee or for commercial purposes, or modification of the content of the paper are prohibited.

Control over wettability via surface modification of porous gradients

Y. L. Khung[a], M. A. Cole[b], S. J. P. McInnes[a] and N. H. Voelcker[a]

[a] School of Chemistry, Physics and Earth Sciences, Flinders University, Adelaide, SA, Australia
[b] Ian Wark Research Institute, University of South Australia, Adelaide SA, Australia

ABSTRACT

The control over surface wettability is of concern for a number of important applications including chromatography, microfluidics, biomaterials, low-fouling coatings and sensing devices. Here, we report the ability to tailor wettability across a surface using lateral porous silicon (pSi) gradients. Lateral gradients made by anodisation of silicon using an asymmetric electrode configuration showed a lateral distribution of pore sizes, which decreased with increasing distance from the electrode. Pore sizes were characterised using scanning electron microscopy (SEM) and atomic force microscopy (AFM). Pore diameters ranged from micrometres down to less than 10 nanometres. Chemical surface modification of the pSi gradients was employed in order to produce gradients with different wetting or non-wetting properties. Surface modifications were achieved via silanisation of oxidised pSi surfaces introducing functionalities including polyethylene glycol, terminal amine and fluorinated hydrocarbon chains. Surface modifications were characterised using infrared spectroscopy. Sessile drop water contact angle measurements were used to probe the wettability in regions of different pore size across the gradient. For the fluorinated gradients, a comparison of equilibrium and dynamic contact angle measurement was undertaken. The fluorinated surface chemistry produced gradients with wettabilities ranging from hydrophobic to near super-hydrophobic whereas pSi gradients functionalised with polyethylene glycol showed graded hydrophilicity. In all cases investigated here, changes in pore size across the gradient had a significant effect on wettability.

KEYWORDS: Wettability, porous silicon, lateral gradients, silanisation

1. INTRODUCTION

The solid-liquid interface is important in defining the degree of wettability (hydrophobicity/hydrophilicity) of a surface and subsequent interactions between the surface and components in the liquid contacting the surface. For example, the increasing demand for sophistication on biochip surfaces has motivated extensive studies of liquid-surface interaction [1, 2]. It is important to note that biochip and material design usually involves tuning of wettability using surface chemistry [3-6] and in particular surface roughness [7, 8] or a combination of texture and chemistry [9, 10]. Surface wettability is a key factor in mediating fluid transport in confined spaces and across surfaces and it also influences adsorption of biomolecules and subsequent biological response. Therefore, control over wettability has significant applications in areas such as biomedical diagnostics and biomaterials.

In recent years, considerable attention had been directed towards self assembled monolayers (SAMs) and polymers with different wettability profiles to influence and modulate the levels of protein adsorption[11]. However it should be noted that wettability is not the only factor mediating protein adsorption. The latter is also susceptible to electrostatic effects and thus is sensitive to the pH of solution and protein isoelectric point [12].

Commonly used methods for tailoring wettability include introduction of chemical moieties on the surface and micro/nano fabrication of patterned and textured surfaces [13]. Generally for smooth flat surfaces a maximal water contact angle of around 110º - 120º is attainable [9, 14, 15]. Beyond this, roughening or surface structuring is required for an increase in contact angle [8, 9]. A well-known example is the so called Lotus effect where surface topography of the hydrophobic lotus leaves and other plant surfaces enable contact angles of >150º and low sliding angles [16].

Whilst many studies have focused on the engineering of surfaces to mimic nature and on the effects of topography and chemistry, the mechanisms involving the simultaneous effects of both chemical and topographical modification on

BioMEMS and Nanotechnology III, edited by Dan V. Nicolau, Derek Abbott, Kourosh Kalantar-Zadeh, Tiziana Di Matteo, Sergey M. Bezrukov, Proc. of SPIE Vol. 6799, 679909, (2007) · 0277-786X/07/$18 · doi: 10.1117/12.759377

Archived at Flinders University: dspace.flinders.edu.au

wettability are not completely understood [17]. However, with further research directed towards this area, applications in biodevices and microfluidic systems stand to benefit from fabrication schemes involving methods for tailoring wettability on surfaces.

Recent studies have favoured the preparation of surfaces with a continuously varying chemical composition along one direction or dimension on the surface [17, 18]. The chemical gradient systems produce surfaces with varying properties in wettability, polymer thickness and other physicochemical aspects across one dimension. The advantages conferred in such systems have found use in controlled motion of droplets on surfaces as well as selective biomolecule adsorption for biomaterial design[19]. With the integration of suitable analytical techniques, gradients are powerful analytical tools for examination of a spectrum of effects within a single sample surface.

Improvements in surface chemistry and fabrication techniques enable us to tailor material surfaces with topographical features spanning from several microns to a few nanometers. Porous silicon (pSi) is one of the most promising candidates for the fabrication of nanostructured surfaces for a wide range of applications [20, 21]. It has been found to be highly biocompatible and biodegradable [22], displays highly tunable optical properties [23] and a surface chemistry that can easily be modified with very stable Si-C (hydrosilylation) or Si-O bonds (silanisation) [20, 24]. pSi is commonly fabricated by electrochemical anodic etching of silicon wafers in the presence of hydrofluoric acid. Dimensions of the porous micro-architecture and the thickness of the porous layer from the wafer can be varied with the anodic etching current density in x,y direction and the time of anodisation in the z direction.

The correlation of pore size and current density also render pSi attractive as a candidate for studying gradients. The possibility to fabricate pSi surfaces containing a distribution of pore sizes by anodisation in an asymmetrical arrangement has been described previously [25]. The current within the electrolytic solution varies as a function of distance of the electrode to the counter electrode due to resistance of the electrolyte, thus leading to a decrease in current density as the distance from the electrode increases [25, 26]. This dependence can be exploited to generate a surface displaying a gradient of pore features ranging from large (1-3 μm) to small (5 nm) on a single surface [27]. Modification of the applied anodic current can control the size range of these pores. So far, such lateral gradients have been utilised for the fabrication of optical band filters [28] and for studies of biomolecule adsorption [29].

On a typical flat surface, the main influencing factor on wettability will be the nature of the surface chemistry and surface energies. As surface energy is lowered, the hydrophobicity and thus the water contact angle of a surface increases [15]. When a porous surface is introduced in concert with appropriate surface chemistry, the resulting contact angle on the surface will be the net of both factors. Under certain conditions Cassie-Baxter or Wenzel wetting behaviour is observed [8]. Whilst the Cassie-Baxter model assumes that a water droplet rests only on top of the surface features without filling pores, Wenzel's model assumes that the surface structure is filled by the water [8].

Here, we have generated pSi gradients to study the effects of pore size on surface wettability using lateral pSi gradients in conjunction with a range of chemical modifications applied to the porous layer.

2. METHOD

2.1 Electrochemical anodisation

pSi samples were prepared from p-type (boron-doped) silicon wafers with (100) orientation and resistivity of 0.0005-0.001 Ω cm (Virginia Semiconductors). Samples were prepared in the setup similar to that as previously described [15]. Briefly, surfaces were etched by placing the electrode perpendicular to the surface on one end of a Teflon well in a 1:1 (v/v) solution of 49 % aqueous HF/ethanol for 90 seconds at a constant current density (Fig. 1a). Three currents were applied: 40 mA, 50 mA and 60 mA over a surface area of 1.767 cm^2, giving current densities of 22.64 mA/cm^2, 28.31 mA/cm^2 and 33.40 mA/cm^2, respectively. After etching, the samples were rinsed with methanol, acetone and dichloromethane and dried under a stream of N_2. The freshly etched pSi surfaces were thermally oxidised in a tube furnace at 600 °C for 1 h or ozone oxidised using a Fischer OZON Ozon-Generator 500 for 20 minutes at ozone rate of 3.25 g h^{-1}. After oxidation, the surfaces were rinsed extensively with ethanol and dried under a stream of N_2.

Archived at Flinders University: dspace.flinders.edu.au

2.2 Silanisation

Surface modification was achieved via silanisation of the thermally oxidised pSi samples using dry distilled solvent and silanes as received.

Surface modification with N-(triethoxysilylpropyl)-O-polyethylene oxide urethane (PEGS) (Gelest Inc) was achieved by submersion of thermally oxidised pSi in anhydrous toluene with a silane concentration of 50 mM at a temperature of 70 ^{o}C for 16 h. Modification with 3-aminopropyl triethoxysilane (APTES) (Aldrich, 98 %) was carried out with 50 mM silane in toluene at 25 ^{o}C for 4 h.

Ozone oxidised pSi was silanised with heptadecafluoro-1,1,2,2-tetrahydrodecyl dimethylchlorosilane (HDFS) (Gelest Inc) and pentafluorophenyl dimethylchlorosilane (PFPS) (Gelest Inc) via flooding the pSi surfaces with the neat chlorosilane followed by incubation in an 80 ^{o}C oven for 15 minutes. After silanisation the surfaces were rinsed with acetone and dichloromethane before being dried under a stream of N_2.

2.3 Scanning electron microscopy

Scanning electron microscopy (SEM) was performed on a Phillips XL30 field emission scanning electron microscope with an acceleration voltage of 10 kV and a capture angle of 90 and 45 degrees relative to the surface.

2.4 Atomic force microscopy

Atomic force microscopy (AFM) images of pSi were acquired on a Nanoscope IV Multimode microscope (Veeco Corp.) operating in tapping mode using silicon tips (FESP, Digital instruments) with a resonance frequency of 50-70 kHz. Image processing was done using Nanoscope v5.12 software. Analysis was performed in the centre of the respective bins shown in figure 1b.

2.5 Infrared spectroscopy

All Infrared (IR) spectra were obtained using a Nicolet Avatar 370MCT from Thermo Electron Corporation equipped with a Smart Diffuse Reflectance Accessory in diffuse reflectance mode (DRIFT). The DRIFT spectra were recorded and analysed using OMNIC version 7.0 software. Spectra were obtained in the range of 650-4000 cm^{-1} at a resolution of 1 cm^{-1}. All spectra were blanked using an unetched silicon wafer of the same type.

2.6 Contact angle measurements

To investigate the surface wettability of modified pSi gradients at regions of different pore size, sessile drop water contact angles were characterised in terms of advancing and static (equilibrium) contact angles. Contact angle experiments were conducted under ambient conditions.

A custom built sessile drop apparatus with an Olympus SZ-PT microscope and lens system mated to a Sony CCD camera was employed. A 10 μL syringe (Hamilton, Reno, USA) was used to dispense droplets of 18.2 MΩ.cm MilliQ (MQ) water of approximately 1 μL to three pore size regions (bins). A minimum of three contact angle measurements were taken from each of the binned regions as described below. Angle analysis of captured droplets was performed with ImageJ software v1.34 (http://rsb.info.nih.gov/ij/).

Archived at Flinders University: dspace.flinders.edu.au

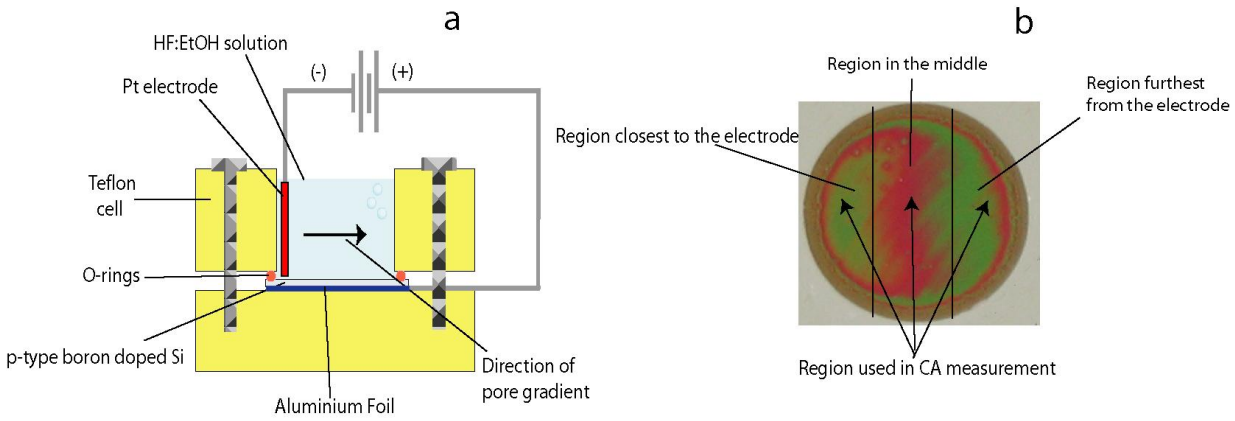

Figure 1: (a) Schematic of setup for production of pSi gradients. (b) Photograph of a pSi gradient with three pore size regions used for sessile drop water contact angle measurements.

3. RESULTS AND DISCUSSION

3.1 Lateral anodisation

Graded pSi surfaces were produced using three different etching current, 40 mA, 50 mA and 60 mA in an asymmetric electrode configuration. The schematic of the setup is as shown in figure 1a. We used three different etching conditions in order to fabricate a spectrum of pore sizes for the wettability studies ranging from micron to nanometer size. A low concentration of HF was selected since this electrolyte gave mechanically stable pores across the whole gradient. The size of surface pores had to be sufficiently large enough to present substantial topographic disparity in conjunction with the chemical modification. A surface topography within the nanometer range may not exert sufficient physicochemical effects on wettability. The physical appearances of the laterally etched pSi surface that we obtained were found to be similar to those previously attained by Sailors group [25]. For all currents used in this work we were able to avoid electropolishing the surface. However, any further increase in the etching current resulted in the loss of porous structure due to electropolishing.

3.2 Surface topography

The topography of the graded pSi films was first characterised using atomic force microscopy (AFM). For this purpose, pSi films etched at the three different currents were divided into different regions as shown in figure 2. The region nearest to the Pt electrode would be expected to yield the largest pore sizes due to the largest electrical field. Pore size/diameter is expected to decrease with increasing distance from the Pt electrode.

Figure 2 shows the AFM analysis from the each of the different selected regions of interest from the laterally etched pSi. At the largest pore region attained from our anodisation as shown in figure 2a, the pore sizes were found to span between 1000-3000 nm. The region with the smallest pores, obtained from the sample etched at 40 mA etching current, displayed 5-20 nm pore sizes (figure 2f). We decided to use six different regions from the three pSi samples corresponding to six different pore size bins to facilitate the wettability measurement. The pore regions selected for contact angle analyses were 1000-3000 nm, 300-1000 nm, 100-300 nm, 50-100 nm, 20-50 nm and 5-20 nm. This binning method is coarse enough to allow the use of fiducial markers to identify the pore region during contact angle measurements, while providing a significant change in pore size between each region. Although finer binning could have been employed, the six chosen pore regions covered the highest pore size (3000 nm) to the smallest pore size (5 nm) and provided a starting point for evaluating the effect of pore size on wettability of the surface.

Archived at Flinders University: dspace.flinders.edu.au

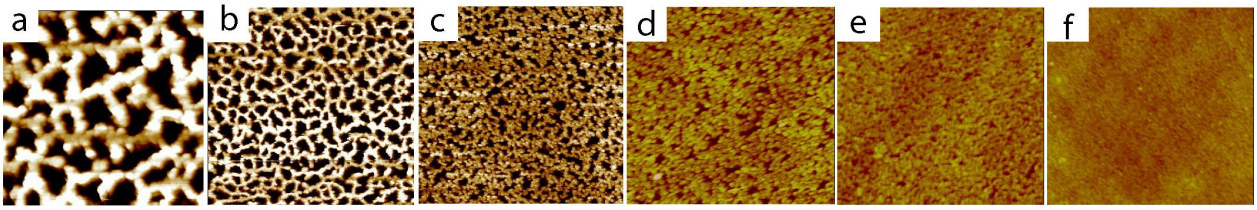

Figure 2: AFM images of lateral pSi gradients displaying pore sizes at the six selected pore size region (a) 1000-3000 nm (b) 300-1000 nm (c) 100-300 nm (d) 50-100 nm (e) 20-50 nm and (f) 5-20 nm. Lateral scale for (a-c) is 5 μm while (d-f) is 2 μm. The z-scale for (a) is 200 nm; (b-c) 50 nm; (d-f) is 10 nm.

The relation between the current density used during anodisation and the pore size observed on the surface is as shown in table 1. In general, sizes of pores on the surface were found to be dependent on the distance from the electrode and the level of anodising current applied. The region closest to the electrode was found to have the largest pores while pores were smallest in regions furthest from the electrode.

Table 1. Pore size distribution on pSi gradients produced at 40-60 mA.

Etching current	***Pore size region***		
	Closest to Pt electrode	*In the middle of pSi surface*	*Furthest from the Pt electrode*
40 mA	50-100 nm	20-50 nm	5-20 nm
50 mA	300-600 nm	100-300 nm	30-100 nm
60 mA	1000-3000 nm	300-1000 nm	700-300 nm

Scanning electron microscopy was performed on all the surfaces to investigate the layer thickness and to further visualise the three dimensional features of the pSi surface that cannot be probed by AFM. Characterisation of the prepared surface structures is important due to the strong influence of topography over the contact angles in conjunction with the chemical silanisation. Figure 3a-c shows the scanning electron micrographs of surfaces produced at 40, 50 and 60 mA respectively. The thickness of the porous layer was determined to be 2.5 μm from figure 3d which was taken at a viewing angle of 45 degrees. It is also interesting to note that smaller pore structures were clearly visible along the bottom of the large pores for the 60 mA samples (figure 3e). It is conceivable that this layer of smaller pores also influences wettability, in particular for Wenzel surfaces where the water probes the interior of the pore.

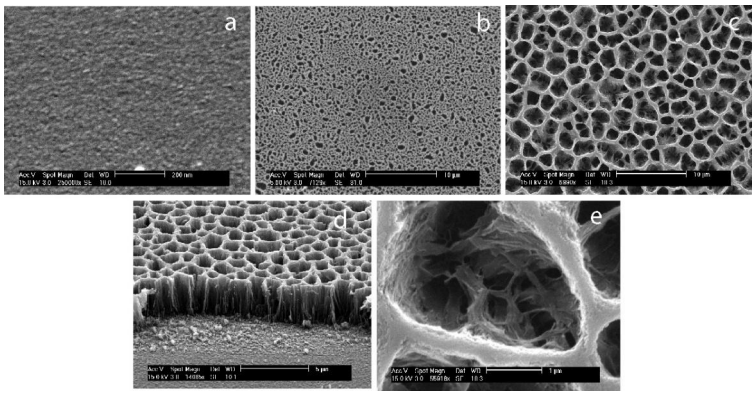

Figure 3: Scanning electron micrographs of gradients for (a) 40 mA, (b) 50 mA, and (c) 60 mA. (d) Profile of pSi layer produced at 60 mA showing a thickness of approximately 2.5 μm. (e) Honeycomb-like microstructures found within individual pores for 60 mA current density. All images are taken from the region nearest to the Pt electrode.

Archived at Flinders University: dspace.flinders.edu.au

3.3 Surface modifications

pSi gradients were oxidised to produce a surface that is stable when in contact with aqueous media [27]. Thermally oxidised pSi was silanised with the silanes N-(triethoxysilylpropyl)-O-polyethylene oxide urethane (PEGS) [24] and with 3-aminopropyl trimethoxysilane (APTES) [21] to produce two hydrophilic organic coatings. On the other hand, ozone oxidised pSi was silanised with fluorinated silanes heptadecafluoro-1,1,2,2-tetrahydrodecyl dimethylchlorosilane (HDFS) and pentafluorophenyl dimethylchlorosilane (PFPS) to produce two hydrophobic coatings [30].

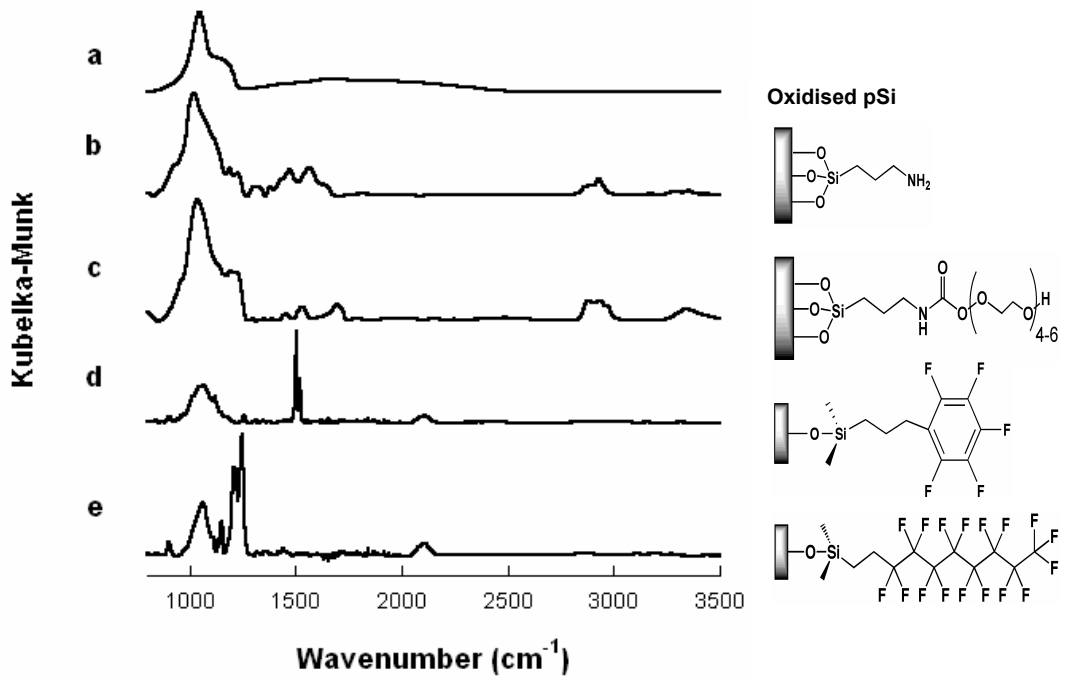

Figure 4: DRIFT spectra of (a) thermally oxidised pSi, (b) APTES silanised pSi, (c) PEGS pSi, (d) PFPS pSi and (e) HDFS pSi. The corresponding surface functionalities are also displayed..

Typical IR spectra for each surface functionalisation are shown in figure 4. Upon thermal oxidation, the laterally etched surfaces (figure 4a) show a characteristic peak at 1080 cm^{-1} corresponding to a Si-O stretching vibration[31]. The APTES pSi surface (figure 4b) displays a large peak at 1080 cm^{-1} for the Si-O stretching as well as a broad peak corresponding to a N-H bending vibration centred at around 1580 cm^{-1}. C-H stretching vibrations at 2850 – 3000 cm^{-1} and a peak corresponding to the bending vibrations at 1460 cm^{-1} are also observed. The PEGS silanised surface (figure 4c) shows a broad peak at around 1080 cm^{-1} for the Si-O and C-O stretching vibrations. The spectrum also shows characteristic peaks at 1460, 1545 and 1710 cm^{-1} for the C-H alkane and N-H amide bending and the C=O stretching vibrations in the amide, respectively. A peak corresponding to C-H stretching vibrations can also be seen at 2850 – 3000 cm^{-1} along with a small peak that stretches across 3400 cm^{-1} this is likely to be caused by the terminal O-H group on the PEGS pSi.

Both the PFPS (figure 4d) and HDFS pSi (figure 4e) surfaces also show peaks centered at 1080 cm^{-1} for the Si-O stretching, and the symmetric stretching vibration of CF_3 [32]. Importantly the PFPS pSi spectrum (Fig. 4d) shows a peak at 1260 cm^{-1} which can be attributed to aromatic C-F stretching and peaks at 1500 cm^{-1} attributed to the C-C in ring stretching vibrations of aromatic systems. The HDFS pSi spectra (figure 4e) clearly shows sharp peaks that can be assigned to CF_2 stretching vibrations at 1150 and 1220 cm^{-1} and the CF_3 asymmetric stretching vibration at 1250 cm^{-1} [32]. Due to the low sensitivity of diffused reflectance IR on laterally graded porous surface, it is hard to observe any C-H stretching vibrations on both the HFDS and PFPS pSi surfaces. However the surface may not be fully covered due to the presence of a small peak at 2100 cm^{-1}, which is representative of Si-H_x stretching vibrations and is indicative of incomplete ozone oxidation.

Archived at Flinders University: dspace.flinders.edu.au

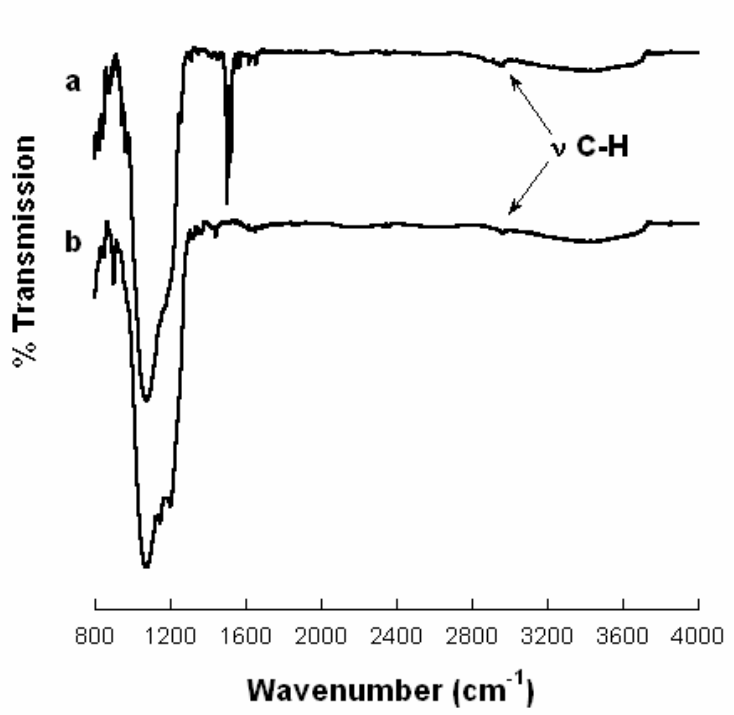

Figure 5: Transmission IR spectra of pSi silanised with (a) PFPS and (b) HDFS.

Due to the low sensitivity of the DRIFTS scans, transmission IR scans were performed in order to visualise the C-H stretches for the short propyl chains and further confirm the effective surface functionalisation with both PFPS and HDFS. In order to facilitate the transmission of the IR beam through the samples, higher resistivity (3-6 Ω cm) boron doped silicon wafers were etched at a current density of 60 mA for 150 seconds, ozone oxidised and silanised with PFPS and HDFS, respectively. The results are shown in figure 5 and the C-H stretch indicated by a peak at 2960 cm^{-1} is visible in these spectra. It is important to note that all the peaks assigned for both PFPS and HDFS from the DRIFT spectra (figure 4d-e) were also visible in transmission mode IR as expected. The large peak at 1080 cm^{-1} is attributed to the Si-O stretching vibration from the surface and is much more prominent on these surfaces, whilst the Si-H vibrations are absent in the spectra, indicating complete ozone oxidation.

3.4 Water contact angle measurements

Static water contact angles were determined on pSi gradients with the surface modifications as shown in figure 4 to study the effect of pore size on wettability for hydrophilic (PEGS and APTES pSi) and hydrophobic (PFPS and HDFS pSi) coatings. The results are shown in figure 6 and 7.

Figure 6 shows digital photographs of 1µl water droplets on three pore size regions, 300-1000 nm, 100-300 nm and 5-20 nm on PEGS, PFPS and HDFS pSi. The fluorinated surfaces PFPS and HDFS pSi demonstrate low wetting in general and an increased beading of the water with increasing pores size (figures 6a-c and 6d-f).

Archived at Flinders University: dspace.flinders.edu.au

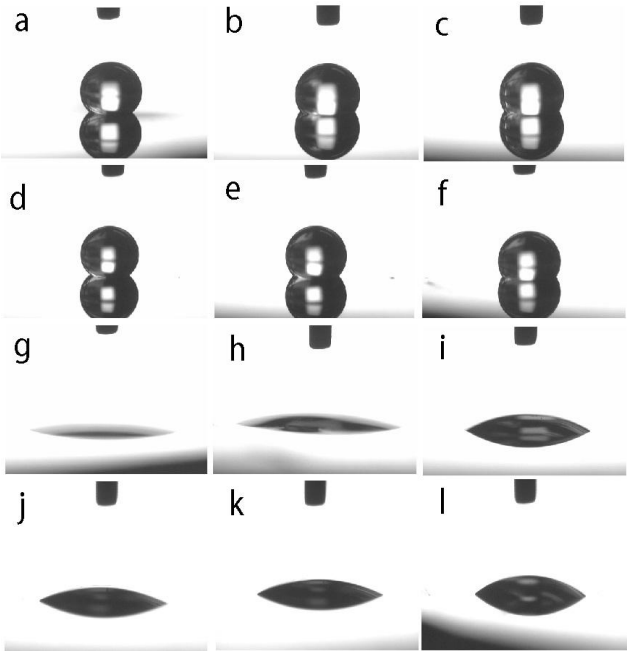

Figure 6: Photographs of static water contact angle measurements performed on different surfaces corresponding to three binned pore size regions, with the largest pores from the left to the smallest pores from the right for PFPS (a) 1000-3000 nm, (b) 100-300 nm and (c) 5-20 nm, for HDFS on (d) 1000-3000 nm, (e) 100-300 nm and (f) 5-20 nm, for PEGS on (g) 1000-3000 nm, (h) 100-300 nm and (i) 5-20 nm and for ATPES (j)1000-3000 nm, (k) 100-300 nm and (l) 5-20 nm. PEGS and APTES functionalised surface shows an increase in contact angle with decreasing pore size while both PFPS and HDFS pSi displayed a reverse trend.

The hydrophilic PEGS functionalisation shows the reverse trend to the fluorinated porous surfaces with droplet flattening as pore size increases. Therefore in all cases studied here, the larger pore sizes enhance the effects of the applied surface chemistry.

Figure 7 shows the average static water contact angles for the six pore size regions in figure 2. The fluorosilanes produced hydrophobic surfaces with contact angles in excess of 112º (figure 7a). Small standard deviations of less than 2.5º for both PFPS and HDFS coatings are indicative of homogenous coatings. A difference of approximately 11º is observed for the between the smallest and largest pore sizes for both PFPS and HDFS pSi. Values for HDFS pSi are slightly larger than for PFPS pSi which is within expectations as the surface energies for a HDFS coating displaying a terminal CF_3 group is lower than for a PFPS coating [33]. The highest contact angles (around 125º) were observed on the micron size pore regions. On the 5-20 nm pore region, the contact angles were around 113º. In contrast, the static contact angle on flat Si modified with PFPS and HDFS was 90º and 100º respectively, which is significantly lower than the values obtained on the mesoporous region (5-20 nm).

It is a well established fact that surface roughness and topography on an already hydrophobic surface can augment hydrophobicity further [34-36]. The trend we observed on the fluorinated surfaces as described above shows a decrease in contact angle from the largest pores to the smallest one. Based on the Cassie-Baxter model, the contact angle on a composite surface composed of solid material and air (e.g. a porous surface) increases when the fraction of the liquid-air interfacial area increases [37]. The larger the pores, the higher the fraction of liquid-air interfacial area. This model therefore explains well the trend observed here. Previous studies on porous fluoropolymer films templated by silica colloidal assembly within the same pore regime show comparable trends [38]. Our failure to attain superhydrophobicity could be due to the incomplete coverage of the fluorosilanes on the surface and this will be addressed in future work. Interestingly, earlier studies on chemically modified CF_3 flat surfaces were only able to achieve a contact angle of 120º [33, 39], while here the lateral gradient has clearly demonstrated the enhancement of hydrophobicity by means of graded surface roughness.

Archived at Flinders University: dspace.flinders.edu.au

A difference in contact angle of 27º between the smallest and largest pore size regime was observed for the PEGS functionalised gradients (figure 7b). The lowest contact angle observed was 17º (on the 1000-3000 nm region) and the largest 44º (on the 5-20 nm region). These results indicate that the hydrophilic coating allows the water droplet to fill the internal volume of the porous structure observed in figures 2 and 3. Investigation of the static contact on flat Si modified with PEGS showed a slightly higher contact angle of 47º, which is consistent with the trend observed. Whilst APTES functionalised surfaces follow the same trend as PEGS pSi, the change in contact angle is less pronounced. A difference of 9º between the smallest and largest pore size areas for the APTES samples is observed. The standard deviation of contact angles is larger for the APTES functionalised surfaces, perhaps due to a more inhomogenous coating. APTES has a tendency to form a polycondensed multilayer [40]. Taking the large standard deviation into account, it can be concluded that the pore size changes do not as strongly influence wettability of APTES pSi as compared to the PEGS surfaces.

The wettability trend on the hydrophilic porous gradient can be explained by the Wenzel model. In this model, if a porous microstructure is readily invaded by water, an increase in the solid-liquid surface area (e.g. by decreasing pore size) will augment hydrophobicity because of an increase in surface energy of the porous surface [38]. An increase in the absorbed volume of water (e.g. by increasing pore size) however leads to an increased hydrophilicity. Surface silanisation with PEGS and APTES creates hydrophilic surfaces which should allow the penetration of the water droplets into the pores. The larger the pore volume, the more water of the droplet can be absorbed into the porous surface (nanowicking) [41-43]. This explains the observed increase in wettability for increasing pore sizes.

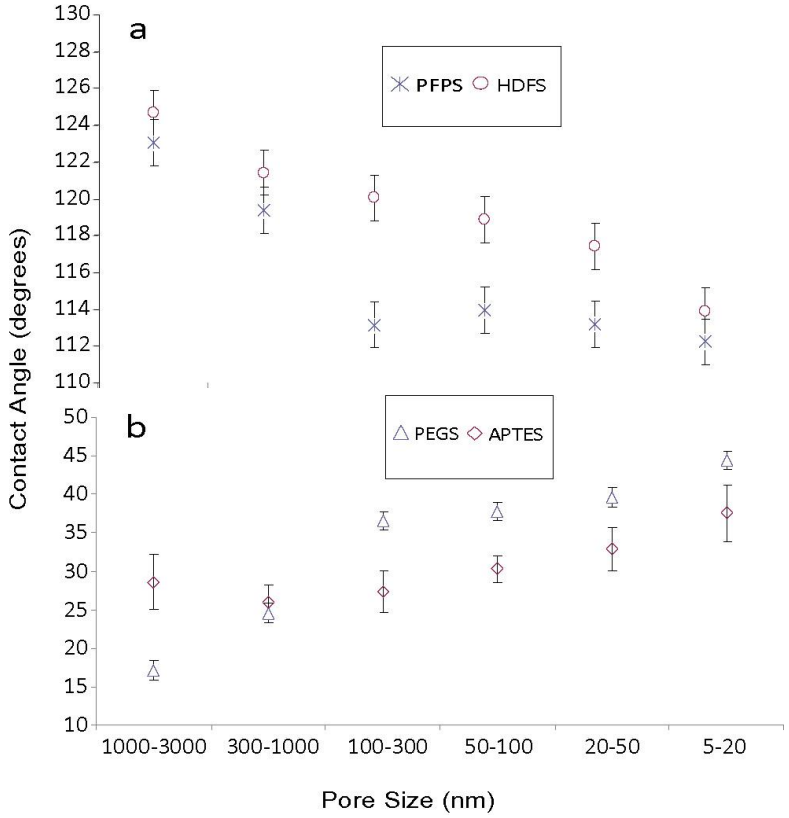

Figure 7. Static water contact angle on (a) PFPS or HDFS functionalised pSi gradients and (b) PEGS or APTES functionalised pSi gradients. The change in contact angle over the lateral gradient on hydrophilic surfaces for PEGS and APTES was 27º and 9º, respectively. The changes on hydrophobic silanes for both PFPS and HDFS were found to be relatively similar, at approximately 11º.

When dynamic advancing contact angles were measured for the hydrophobic surfaces (PFPS and HDFS), a stronger dependence of the wettability on the pore size was observed. Figure 8 shows the advancing contact angle for the HDFS

Archived at Flinders University: dspace.flinders.edu.au

functionalised samples. It can be seen that the difference between the maximal 147º and minimal 114º contact angle values for the largest and smallest pore sizes respectively is now 33º whilst the static contact angle difference was only 11º. This difference between the advancing and static contact angles is clearly caused by the introduction of a porous layer (surface roughness) [33] as the advancing contact angle of flat Si sample modified with HDFS (98º) is very close to the static contact angle of HDFS on flat Si (100º). The upper value of 147º is now approaching the superhydrophobic regime, which is usually defined as a regime of contact angles in excess of 150º [35].

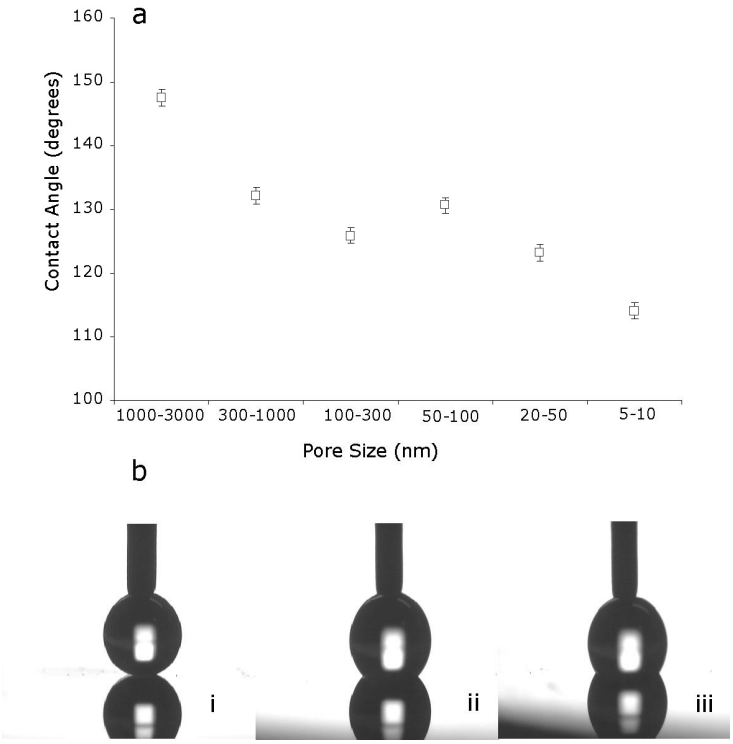

Figure 8: (a) Graph of advancing water contact angle measurements on HDFS functionalised pSi. (b) Photographs of advancing water contact angle experiments performed on (i) 1000-3000 nm, (ii) 100-300 nm and (iii) 5-20 nm pore size regions of HDFS functionalised pSi. The change in contact angle between the largest and the smallest pore region is 33º.

The fluorinated pSi gradients showed a contact angle hysteresis of 22º. The large contact angle hysteresis is indicative of a strong pinning of the liquid-solid contact line and a 'sticky' hydrophobic surface [44-45]. At this point, we are uncertain about the reasons for the large hysteresis. It may be a consequence of the graded nature of the surface or may be related to the dispersity of the pore size and shape. Future investigations will focus on this contact angle hysteresis and its modulation.

4. CONCLUSIONS

We have developed gradients with micro/nano structured surface features which are amenable to surface functionalisation via silanisation. Lateral pSi gradients were prepared by an electrochemical etching procedure using an asymmetric electrode configuration. Simple one step surface modifications of the pSi using silane chemistry afforded surfaces with a range of wettabilities as probed by the sessile drop water contact angle from less than 20º to approximately 150º. For a given surface chemistry, pore size changes of these pSi gradients result in shifts of water contact angle of around 30º.

Depending on the surface chemistry, we have attributed these wettability behaviours to the Wenzel or the Cassie-Baxter model. With further utilisation of both models, we have also managed to determine the relationship between pore size and wetting behaviours on porous substrates.

Archived at Flinders University: dspace.flinders.edu.au

Hence, using this gradient format, one can identify desired wettability regimes on a single sample therefore reducing analysis and preparation cost and time. The format is also suitable for the investigation of biomolecule surface or cell surface interactions with the aim to develop surfaces with desired surface properties for biotechnological applications including biomaterials, biosensors and microarrays.

ACKNOWLEDGEMENTS

The authors gratefully acknowledge financial support from Flinders University and the Australian Research Council. The fluoro silanes were kindly provided by Rachel Lowe.

REFERENCES

1. T. Onda, S. Shibuichi, N. Satoh and K. Tsujii "Super-Water-Repellent Fractal Surfaces". Langmuir **12,** 2125-7 (1996).
2. R. Blossey "Self-cleaning surfaces - virtual realities". Nature Materials **2,** 301-306 (2003).
3. G. Khang, J. Hyeong, J. C. Cho, J. M. Rhee and H. B. Lee "Improvement of wetting property for porous PLGA scaffold by physicochemical treatment". Polymer (Korea) **23,** 861-868 (1999).
4. M. Geoghegan and G. Krausch "Wetting at polymer surfaces and interfaces". Progress in Polymer Science **28,** 261-302 (2002).
5. J. W. Lussi, R. Michel, I. Reviakine, D. Falconnet, A. Goessl, G. Csucs, J. A. Hubbell and M. Textor "A novel generic platform for chemical patterning of surfaces". Progress in Surface Science **76,** 55-69 (2004).
6. M. Riepl, M. Ostblom, I. Lundstrom, S. C. T. Svensson, A. W. D. van der Gon, M. Schaferling and B Liedberg "Molecular gradients: An efficient approach for optimizing the surface properties of biomaterials and biochips". Langmuir **21,** 1042-1050 (2005).
7. L. Zhu, Y. Feng, X. Ye and Z. Zhou "Tuning wettability and getting superhydrophobic surface by controlling surface roughness with well-designed microstructures". Sensors and Actuators, A: Physical **A130-A131,** 595-600 (2006).
8. R. Rosario, D. Gust, A. A. Garcia, M. Hayes, J. L. Taraci, T. Clement, J. W. Dailey and S. T. Picraux "Lotus effect amplifies light-induced contact angle switching". Journal Of Physical Chemistry B **108,** 12640-12642 (2004).
9. X. Yu, Z. Q. Wang, Y. G. Jiang and X. Zhang "Surface gradient material: From superhydrophobicity to superhydrophilicity". Langmuir **22,** 4483-4486 (2006).
10. J. Pacifico, K. Endo, S. Morgan and P. Mulvaney "Superhydrophobic effects of self-assembled monolayers on micropatterned surfaces: 3-D arrays mimicking the lotus leaf". Langmuir **22,** 11072-11076 (2006).
11. F. Fang and I. Szleifer "Effect of molecular structure on the adsorption of protein on surfaces with grafted polymers". Langmuir **18,** 5497-5510 (2002).
12. N. Nath, J. Hyun, H. Ma and A. Chilkoti "Surface engineering strategies for control of protein and cell interactions". Surface Science **570,** 98-110 (2004).
13. F. Xia, L. Feng, S. T. Wang, T. L. Sun, W. L. Song, W. H. Jiang and L Jiang "Dual-responsive surfaces that switch superhydrophilicity and superhydrophobicity". Advanced Materials **18,** 432-+ (2006).
14. G. McHale, N. J. Shirtcliffe and M. I. Newton "Contact-angle hysteresis on super-hydrophobic surfaces". Langmuir **20,** 10146-10149 (2004).
15. A. Nakajima, K. Hashimoto and T. Watanabe "Recent Studies on Super-Hydrophobic Films". Monatshefte fur Chemie **132,** 31-41 (2001).
16. W. Barthlott and C. Neinhuis "Purity of the sacred lotus, or escape from contamination in biological surfaces". Planta **202,** 1-8 (1997).
17. T. G. Ruardy, J. M. Schakenraad, H. C. van der mei and H. J. Busscher "Preparation and characterization of chemical gradient surfaces and their application for the study of cellular interaction phenomena". Surface Science Reports **29,** 1-30 (1997).
18. C. Xu, T. Wu, J. D. Batteas, C. M. Drain, K. L. Beers and M. J. Fasolka "Surface-grafted block copolymer gradients: Effect of block length on solvent response". Applied Surface Science **252,** 2529-2534 (2006).
19. I. Choi, S. K. Kang, J. Lee, Y. Kim and J. Yi "In situ observation of biomolecules patterned on a PEG-modified Si surface by scanning probe lithography". Biomaterials **27,** 4655-4660 (2006).
20. M. P. Stewart and J. M. Buriak "Chemical and biological applications of porous silicon technology". Advanced Materials **12,** 859-869 (2000).
21. S. P. Low, K. A. Williams, L. T. Canham and N. H. Voelcker "Evaluation of mammalian cell adhesion on surface-modified porous silicon". Biomaterials **27,** 4538-4546 (2006).
22. L. T. Canham "Bioactive silicon structure fabrication through nanoetching techniques". Advanced Materials **7,** 1033-& (1995).

Archived at Flinders University: dspace.flinders.edu.au

23. A. Janshoff, K. P. S. Dancil, C. Steinem, D. P. Greiner, V. S. Y. Lin, C. Gurtner, K. Motesharei, M. J. Sailor and M. R. Ghadiri "Macroporous p-type silicon Fabry-Perot layers. Fabrication, characterization, and applications in biosensing". Journal Of The American Chemical Society **120,** 12108-12116 (1998).
24. Y. L. Khung, S. D. Graney and N. H. Voelcker "Micropatterning of porous silicon films by direct laser writing". Biotechnology Progress **22,** 1388-1393 (2006).
25. B. E. Collins, K. P. S. Dancil, G. Abbi and M. J. Sailor "Determining protein size using an electrochemically machined pore gradient in silicon". Advanced Functional Materials **12,** 187-191 (2002).
26. R. Jedamzik, A. Neubrand and J. Rodel "Production of functionally graded materials from electrochemically modified carbon preforms". Journal Of The American Ceramic Society **83,** 983-985 (2000).
27. Y. L. Khung, G. Barritt and N. H. Voelcker "Using continuous porous silicon gradients to study the influence of surface topography on the behaviour of neuroblastoma cells". Experimental Cell Research**,** doi: 10.1016/j.yexcr.2007.10.015 (2007).
28. Y. Y. Li, P. Kim and M. J. Sailor "Painting a rainbow on silicon - a simple method to generate a porous silicon band filter gradient". Physica Status Solidi A-Applications And Materials Science **202,** 1616-1618 (2005).
29. L. M. Karlsson, M. Schubert, N. Ashkenov and H. Arwin "Adsorption of human serum albumin in porous silicon gradients monitored by spatially-resolved spectroscopic ellipsometry". Phys. Status Solidi C: Conferences and Critical Reviews **2,** 3293-3297 (2005).
30. R. Lowe, E. P. Go, G. C. Tong, N. H. Voelcker and G. Siuzdak "Monitoring EDTA and endogenous metabolite biomarkers from serum with mass spectrometry". Spectroscopy-an International Journal **19,** 137-146 (2005).
31. O. Bisi, S. Ossicini and Pavesi, L. "Porous silicon: a quantum sponge structure for silicon based optoelectronics". Surface Science Reports **38,** 1-126 (2000).
32. L. N. Ignatieva, A. K. Tsvetnikov, A. N. Livshits, V. I. Saldin and V. M. Buznik "Spectroscopic Study of Modified Polytetrafluoroethylene ". Journal of Structural Chemistry **43,** 64-68 (2002).
33. T. Nishino, M. Meguro, K. Nakamae, M. Matsushita and Y. Ueda "The Lowest Surface Free Energy Based on -CF3 Alignment". Langmuir **15,** 4321-4323 (1999).
34. J. Bico, U. Thiele and D. Quere "Wetting of textured surfaces". Colloids and Surfaces a-Physicochemical and Engineering Aspects **206,** 41-46 (2002).
35. A. Lafuma, and D. Quere "Superhydrophobic states". Nature materials **2,** 457-60 (2003).
36. D. Oener T. J. McCarthy "Ultrahydrophobic Surfaces. Effects of Topography Length Scales on Wettability". Langmuir **16,** 7777-7782 (2000).
37. R. D. Narhe and D. A. Beysens "Water condensation on a super-hydrophobic spike surface". Europhysics Letters **75,** 98-104 (2006).
38. J. Li, J. Fu, Y. Cong, Y. Wu, L. Xue and Y. Han "Macroporous fluoropolymeric films templated by silica colloidal assembly. A possible route to super-hydrophobic surfaces". Applied Surface Science **252,** 2229-2234 (2006).
39. W. Chen, A. Y. Fadeev, M. C. Hsieh, D. Oener, J. Youngblood and T. J. McCarthy "Ultrahydrophobic and Ultralyophobic Surfaces: Some Comments and Examples". Langmuir **15,** 3395-3399 (1999).
40. J. Y. Zhao, Y. H. Li, H. Q. Guo and L. X. Gao "Relative surface density and stability of the amines on the bio-chip". Chinese Journal of Analytical Chemistry **34,** 1235-1238 (2006).
41. N. J. Shirtcliffe, G. McHale, M. I. Newton, C. C. Perry and P. Roach "Porous materials show superhydrophobic to superhydrophilic switching". Chemical Communications**,** 3135-3137 (2005).
42. F. C. Cebeci, Z. Z. Wu, L. Zhai, R. E. Cohen and M. F. Rubner "Nanoporosity-driven superhydrophilicity: A means to create multifunctional antifogging coatings". Langmuir **22,** 2856-2862 (2006).
43. G. McHale, N. J. Shirtcliffe, S. Aqil, C. C. Perry and M. I. Newton "Topography driven spreading". Physical Review Letters **93** (2004).
44. B. He, J. Lee and N. A. Patankar "Contact angle hysteresis on rough hydrophobic surfaces". Colloids and Surfaces a-Physicochemical and Engineering Aspects **248,** 101-104 (2004).
45. D. Quere, A. Lafuma and J. Bico "Slippy and sticky microtextured solids". Nanotechnology **14,** 1109-1112 (2003).

Archived at Flinders University: dspace.flinders.edu.au